www.springer.com/41230
https://doi.org/10.1007/s41230-025-4075-4
Research & Development
Vol. 22 No. 2 March 2025
CHINA FOUNDRY

Effect of iron content and heat treatment on microstructure and mechanical properties of a recycled Al-Si-Mg aluminum alloy

Sha Lan[1, 2], Gang Feng[2], *Ya-jun Wang[1], Jin-sheng Zhang[1, 2], Fu-jian Gong[2], Chun Wang[1], Jian-hua Zhao[1, 3], Qing Yang[2], and Zhi-bai Wang[2]

1. College of Material Science and Engineering, Chongqing University, Chongqing 400045, China
2. Changan Automobile Co., Ltd., Chongqing 401120, China
3. National Engineering Research Center for Magnesium Alloys, Chongqing University, Chongqing 400044, China

Abstract: The iron content is one of the most critical parameters affecting the microstructure and mechanical properties of recycled aluminum alloy. This study aimed to compare the microstructure and tensile properties of alloys with varying iron content to ascertain the optimal iron content for formulating a recycled Al-Si-Mg aluminum alloy. Additionally, the effects of aging temperature and aging time on the microstructure and mechanical properties of recycled aluminum alloy were investigated. With increasing aging temperature and time, both tensile strength and yield strength are improved, while elongation is decreased. Specifically, when subject to a heat treatment consisting of a solution treatment at 535 °C for 5 h followed by an aging treatment at 170 °C for 5.5 h, the newly designed recycled aluminum alloy achieves a tensile strength of 291 MPa and a yield strength of 238 MPa. These findings hold significant implications for the further development and broader application of recycled aluminum alloys.

Keywords: recycled aluminum alloy; iron content; heat treatment; microstructure; mechanical property

CLC numbers: TG146.21 **Document code:** A **Article ID:** 1672-6421(2025)02-205-10

1 Introduction

Aluminum alloy, renowned for its exceptional castability, high corrosion resistance, and notably high strength-to-weight ratio in the heat-treated conditions, has garnered increased attention in the automobile industry [1-4]. The recycling of aluminum alloys has emerged as a prominent area of interest in contemporary times due to its environmentally friendly and cost-effectiveness [5-7]. Compared to industrial primary aluminum, scrap aluminum alloys exhibit characteristics such as low melting temperature, short melting time, minimal metal combustion loss, and low energy consumption. During the alloy composition adjustment stage, less metal needs to be added to scrap aluminum alloys, resulting in a more even distribution of alloy constituents and optimized microstructure [8]. Additionally, the energy consumption for producing one ton of recycled aluminum is only about 3%–5% of that for producing primary aluminum, reducing production costs and decreasing the emissions of carbon dioxide and sulfur oxides during the production process. This plays a positive role in conserving resources and protecting the environment [9, 10].

However, during the recycling of aluminum alloys, it is unavoidable that a certain amount of iron will be mixed into the original aluminum alloys [11, 12]. Iron is one of the primary detrimental elements in aluminum alloys. Although the maximum solubility of iron in aluminum is 0.052wt.%, iron often reacts with aluminum alloy to form iron-rich phases, thereby affecting the performance of the alloy. As most of the iron-rich phases exhibit higher microhardness and a coarse acicular morphology, these iron-rich phases can act as stress concentrators in the aluminum alloy matrix, fracturing the integrity of dendritic cells,

***Ya-jun Wang**

Experimentalist. His main research interests lie in high-performance aluminum alloys, magnesium alloys, and their forming technology. He has led and participated in over 13 scientific research projects, contributed to the formulation of 3 national and industry standards, and published more than 20 papers.

E-mail: wyjwyj202305@163.com
Received: 2024-04-11; Revised: 2024-08-07; Accepted: 2024-11-25

thereby severely affecting the mechanical properties of the alloy. Therefore, corresponding process measures are typically employed in actual industrial production to mitigate the impact of the iron-rich phase on the mechanical properties of the alloy. Adding alloying elements has been proven to be an efficacious means of enhancing the mechanical properties and optimizing the microstructural characteristics of Al-Si-Mg aluminum alloys [17, 18].

Sr is commonly used as a modifier during the melting process in aluminum alloy. Adding Sr to Al-Si alloy can increase the undercooling of eutectic nucleation, thus inhibiting eutectic growth and modifying the morphology and size of eutectic silicon. Moreover, the addition of Sr promotes the primary aluminum nucleation in Al-Si alloys, thereby achieving the purpose of refining the primary aluminum phase. This refinement decreases the cleavage effect of the eutectic silicon phase on the aluminum matrix, thereby improving the mechanical properties of recycled aluminum alloys [19-23]. Previous studies [22, 24] have shown that when the Sr content in Al-Si alloys exceeds around 0.02wt.%, it has a favorable modification effect on the eutectic silicon phase within the alloy. Therefore, this investigation opted a Sr content at a level of 0.03wt.%. Mn and Fe have similar atomic radii. By incorporating Mn into the iron-rich aluminum alloy, it is capable of replacing the needle-like β-phase Fe, leading to a transformation of the alloy's iron-rich phase into a Chinese-script-like α-phase [14]. Currently, there is no consensus regarding the optimal amount of Mn to add into iron-rich aluminum alloys. Some believe that the Mn content in the α-Al(Mn,Fe)Si phase is approximately half of the Fe content, suggesting that the amount of Mn added should be half of the Fe content in the alloy. Thus, in this study, the Mn addition amount is set at 0.10wt.%.

Heat treatment is another method that can significantly enhance the mechanical properties of recycled aluminum alloy. Its objective is to foster the formation of the Mg_2Si phase and further refine the morphology of the eutectic Si [17, 23, 25, 26]. During the solution treatment stage, both the Mg_2Si and eutectic Si formed during the casting process dissolve owing to the rise in temperature, leaving the alloy matrix in an oversaturated state. Subsequently, with aging treatment, the precipitate of the Mg_2Si strengthening phase disperses within the aluminum matrix, while the eutectic silicon phase transforms into a nearly spherical shape. Pramod et al. [21] reported that following T6 heat treatment, the morphology of eutectic Si changed to fibrous in A356 alloy and globular in Sc-added A356 alloy. Bayraktar et al. [27] found that T6 heat treatment in Al-12Si-0.6Mg alloy resulted in solid solution hardening (Mg_2Si), refinement of δ and π phases, spheroidization of eutectic silicon crystals, and partial rounding of the edges of primary silicon crystals. Aging treatment parameters play a crucial role in affecting the mechanical properties of the alloy. Zheng et al. [28] observed enhanced mechanical properties in the Al-Mg-Si alloy as aging time increased from 2 h to 6 h, peaking at 6 h. However, surpassing 6 h of aging led to a decline due to over-aging. Geetha et al. [29] explored the influence of aging temperature (100 °C, 200 °C, 300 °C, and 400 °C) on the mechanical properties of A356 alloy, noting an initial increase followed by a decrease in ultimate strength values. In our investigation, the aging temperature ranged from 140 °C to 170 °C, while the aging time ranged from 3.5 h to 5.5 h.

Existing research has predominantly focused on high-iron-content aluminum alloys [ω(Fe) ≥ 0.5wt.%], with relatively less attention given to low-iron-content aluminum alloys where ω(Fe) ≤ 0.4wt.% [6, 30, 31]. Additionally, within low-iron-content aluminum alloys, there exists a more diverse range of iron-rich phases, highlighting their significant research value. Therefore, in this study, the three alloys with iron content of 0.2wt.%, 0.3wt.%, and 0.4wt.% were investigated. Through comparative analysis of metallographic microstructure observation and tensile performance, the optimal iron content for a new recycled Al-Si-Mg aluminum alloy was determined. Based on this iron content, a suitable amount of Sr element and Mn element was added. Additionally, the effects of different aging times and temperatures in the T6 heat treatment process on the microstructure and mechanical properties of this alloy were investigated. Tensile tests were conducted to obtain mechanical properties, including tensile strength, yield strength, and elongation of the alloy. This investigation provides valuable heat treatment parameters for the industrial production of the new recycled aluminum alloy.

2 Materials and experiment

The experimental raw materials comprised high-purity aluminum (99.99% purity), Al-Si intermediate alloy (Si content: 15.01wt.%), pure magnesium (99.99% purity), Al-Fe intermediate alloy (Fe content: 10.75wt.%), and Al-Ti-B refiner (Ti content: 5.01wt.%; B content: 0.97wt.%). This study aimed to explore the impact of varying iron content (0.2wt.%, 0.3wt.%, and 0.4wt.%) on the microstructure and properties of recycled aluminum alloy. Al-10Sr and Al-80Mn intermediate alloy were introduced after the optimal iron content was determined.

The SPZ-25 type melting furnace with a handheld thermocouple temperature controller was heated to 745 °C to melt the alloys. The melt was stirred evenly, degassed with argon gas (99% purity) for 10 min, and the furnace scum was scooped away before pouring into the mold preheated to 200 °C. The alloys with different iron content were subjected to chemical composition analysis by means of XRF-1800 X-ray fluorescence spectrometer. The test results are presented in Table 1.

Specimens utilized for microstructure observation were obtained from the castings. Subsequently, a preparation process involving sandpaper polishing and diamond polishing paste treatment, followed by corrosion treatment using a 0.5wt.% HF solution was carried out. Metallographic microstructure was observed using a Zeiss Axio Vert. A1 optical microscope, and SEM images were captured using a TESCAN tungsten

Table 1: Chemical composition of the three alloys with different iron content (in wt.%)

Alloy	Si	Mg	Fe	Ti	Al
Alloy 1 (0.2wt.% Fe)	6.86	0.36	0.18	0.12	Bal.
Alloy 2 (0.3wt.% Fe)	6.75	0.39	0.32	0.14	Bal.
Alloy 3 (0.4wt.% Fe)	6.52	0.32	0.37	0.14	Bal.

filament scanning electron microscope. Standard tensile samples, measuring 30 mm in length and 12 mm in diameter, were machined from the castings, with three specimens of each alloy taken for testing.

By comparing the microstructure and tensile properties of alloys with three different iron content, the optimal iron content can be determined. Subsequently, the newly designed alloy, which incorporated Al-Sr and Al-Mn intermediate alloys, underwent a T6 heat treatment, which entailed a solution treatment at 535 °C for 5 h, followed by quenching in cold water. Subsequently, it underwent aging treatments and finally air cooling. Existing research [32] investigated the Al-7Si alloy with a similar Al-Si ratio to that selected for this study, and found that the best mechanical properties were achieved with an aging temperature of 160 °C and an aging time of 5 h. Therefore, for the newly designed aluminum alloy in this study, four different aging temperatures (140, 150, 160, and 170 °C) and three aging times (3.5, 4.5, and 5.5 h) were set to explore the most suitable aging parameters for the recycled aluminum alloy. A MXQ1300-type vacuum furnace was employed in the heat treatment process. Microstructural observations and tensile performance tests were conducted on the specimens after heat treatments.

3 Results and discussion

3.1 Effect of iron content on microstructure and tensile properties

The metallographic microstructure of the three alloys with different iron content is depicted in Fig. 1. The eutectic silicon phase and iron-rich phase grow along the grain boundaries of the aluminum matrix. The eutectic phase, when being unmodified and has not subjected to heat treatment, exhibits block-like and lamellar morphologies. Furthermore, with an increase in iron content, there is a concurrent rise in the precipitation of the eutectic silicon phase within the aluminum matrix. As illustrated in Fig. 1(c), there is a notable aggregation of eutectic silicon phases across a considerable area, leading to significant embrittlement of the aluminum matrix and potentially impacting the tensile properties of the alloy.

In Al-Si-Mg alloys, the iron-rich phase primarily exists in two forms: the β-AlFeSi phase and the π-AlSiMgFe phase. The microstructural morphology of the iron-rich phase varies with the iron content in the alloys, as depicted in Fig. 2. The distinct compositions of phase elements enable clearer differentiation when observed using the backscattered electron mode (BSE) of scanning electron microscopy. Further discrimination of the iron-rich phase in the alloy is achieved through EDS map scanning analysis, based on the distribution of Mg and Fe elements. Since the π-AlSiMgFe phase contains Mg elements, the overlapping regions where Mg and Fe elements coalesce denote the presence of the π-AlSiMgFe phase. Conversely, regions where only Fe elements aggregate correspond to the β-AlFeSi phase. At an iron content of 0.2wt.%, the predominant π-AlSiMgFe phase in the alloy exhibits a distinct morphology of Chinese characters. While, with an iron content of 0.3wt.%, the π-AlSiMgFe phase shows a skeleton-like morphology. As the iron content increases to 0.4wt.%, there is a notable enlargement in the size of the iron-rich phase. In Fig. 2(c), SEM image displays a noticeably larger size of the iron-rich phase compared to that of Fig. 2(b), indicating that the size of the iron-rich phase in the alloy increases with the iron content. Concurrently, observations in the alloy reveal both Chinese character-like or skeleton-like morphologies for the π-AlSiMgFe phase and a needle-like morphology for the β-AlFeSi phase, with intertwining patterns. Lu et al. [33] observed that in Al-Si alloys, when

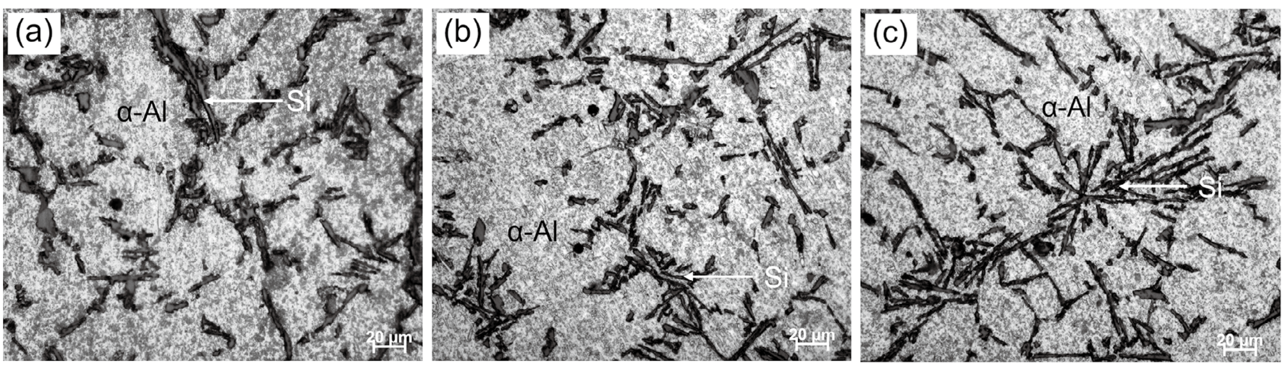

Fig. 1: Microstructures of the three alloys with varing iron content: (a) 0.2wt.% Fe; (b) 0.3wt.% Fe; (c) 0.4wt.% Fe

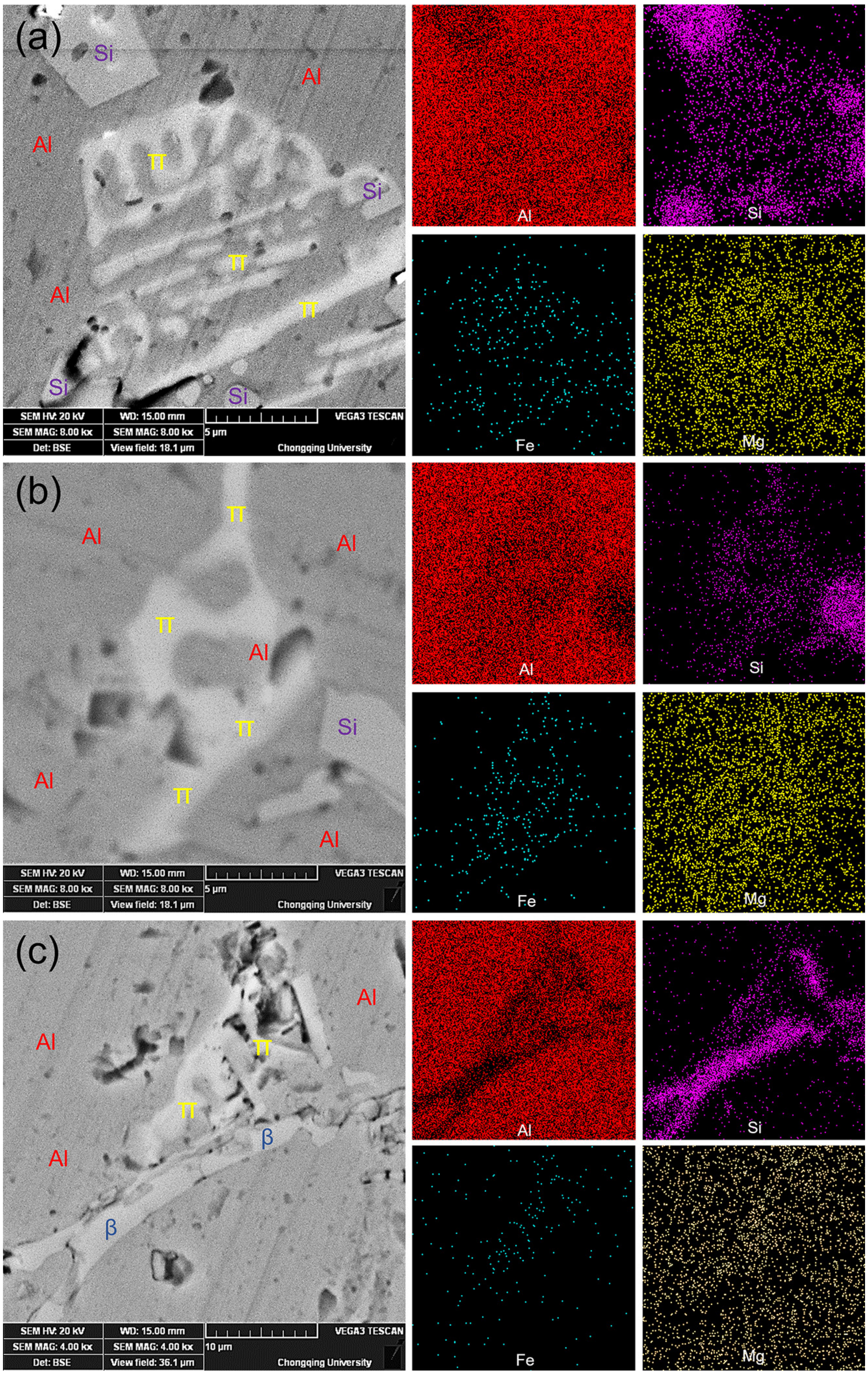

Fig. 2: SEM images and EDS mapping results of iron-rich intermetallics in the three alloys with varing iron content: (a) 0.2wt.% Fe; (b) 0.3wt.% Fe; (c) 0.4wt.% Fe

the iron content exceeds 0.3wt.%, the predominant iron-rich phase primarily manifests as the needle-like β phase. Additionally, there is a gradual proliferation of the needle-like β phase within the alloy as the iron content increases. Sweet et al. [34] also noted that at an iron content of 0.5wt.%, the alloy concurrently exhibits both the needle-like β phase and the Chinese character-like π phase. Furthermore, the intertwined growth between the β phase and π phase was observed.

Figure 3 illustrates the tensile curves of alloys with three different iron content. It is notable that the recycled aluminum alloy does not exhibit a discernible yield point. Consequently, the 0.2% yield strength measurement was utilized for this study. The aluminum alloy with an iron content of 0.2wt.% demonstrates superior tensile strength and elongation, presenting the optimal overall tensile properties. Figure 4 shows a comparison of the specific tensile properties of the three alloys. With an increase in iron content, the tensile strength of the alloy initially decreases before exhibiting an upward trend. The highest tensile strength is observed at an iron content of 0.2wt.%, reaching 152.8 MPa. Conversely, both yield strength and elongation decrease as the iron content rises. At an iron content of 0.2wt.%, the alloy demonstrates an optimal yield strength of 81.9 MPa, marking a 9.4% and 9.8% higher compared to alloys with iron content of 0.3wt.% and

0.4wt.%, respectively. In a study by Karabulut et al. [35], a similar pattern was identified. Within the AlSi7Mg0.3 aluminum alloy, an increase in iron content corresponded to a decrease in tensile strength, yield strength, and elongation. This underscores the proportional reduction in the alloy's tensile properties with higher levels of iron content. Therefore, given the alloy's favorable comprehensive mechanical performance at an iron content of 0.2wt.%, this specific iron content was chosen for further investigation.

Al-Sr intermediate alloy and Al-Mn intermediate alloy were added to the alloy with an iron content of 0.2wt.%. The chemical composition testing result of the new alloy is shown in Table 2.

Figure 5 illustrates the microstructure and the tensile curves of the alloy with an iron content of 0.2wt.%, a Sr content of 0.03wt.%, and a Mn content of 0.1wt.%. It is evident that the as-cast newly designed recycled aluminum alloy exhibits a tensile strength, yield strength, and elongation of 187.2 MPa, 96.7 MPa, and 6.5%, respectively. Compared to the alloy without Sr and Mn addition, the tensile strength, yield strength, and elongation are increased by 18.4%, 15.3%, and 10.8%, respectively. This underscores the significant enhancement effect of Sr and Mn on the alloy.

3.2 Effect of aging treatment on microstructure and tensile properties

The metallographic microstructure of the alloy treated by varing aging times (3.5, 4.5, and 5.5 h) at the same aging temperature of 140 °C is shown in Fig. 6. Figure 7 shows the microstructure of the alloy treated by varing aging temperatures (140, 150, 160, and 170 °C) for the same aging time of 5.5 h. Both Fig. 6 and Fig. 7 distinctly reveal the transformative impact of T6 heat treatment on the morphology of the eutectic

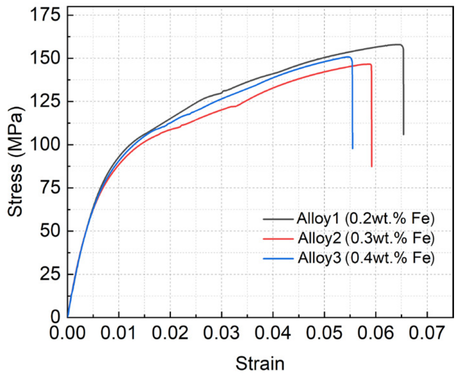

Fig. 3: Tensile stress-strain curves of the three alloys with varing iron content

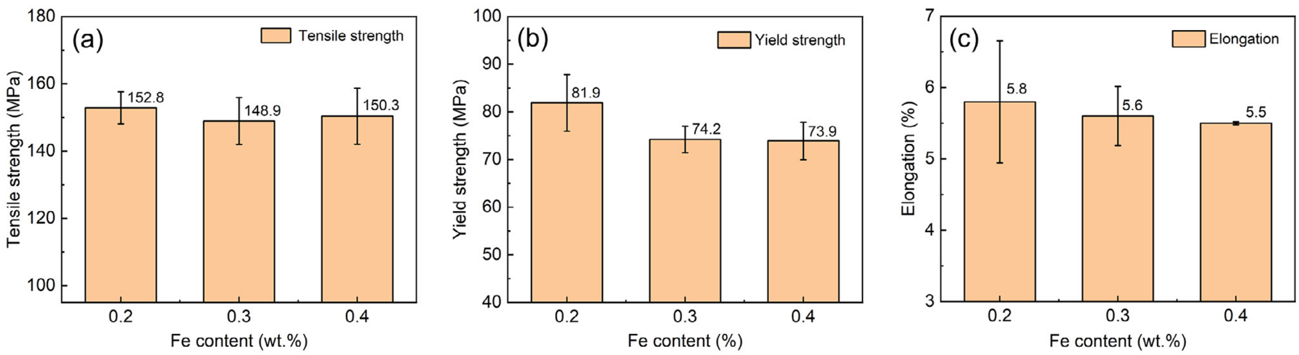

Fig. 4: Variation of tensile strength (a), yield strength (b), and elongation (c) of the alloys with varying iron content

Table 2: Chemical composition of the new recycled aluminum alloy (in wt.%)

Element	Si	Mg	Fe	Ti	Sr	Mn	Al
Designed composition	7.00	0.35	0.20	0.15	0.03	0.10	Bal.
Testing result	6.92	0.31	0.23	0.12	0.035	0.13	Bal.

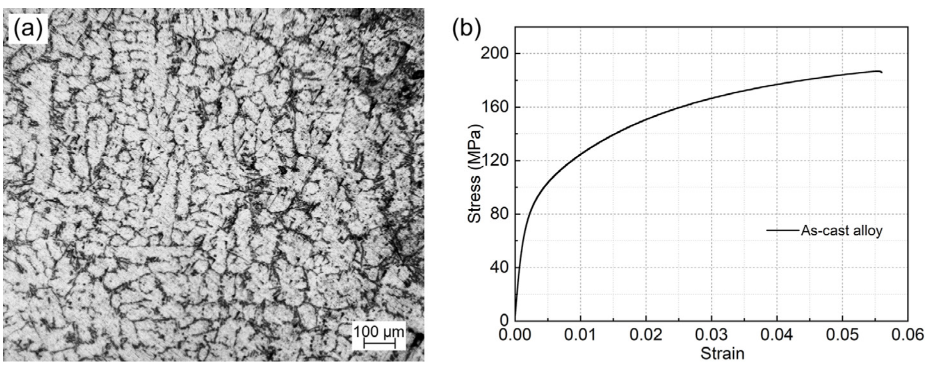

Fig. 5: Microstructure (a) and tensile stress-strain curve (b) of the as-cast newly designed recycled aluminum alloy

silicon structure, transitioning it from its initial lamellar or needle-like configuration to an approximately spherical shape. Notably, absent in these images are any discernible Chinese-character or needle-like iron-rich phases, indicating that heat treatment effectively modifies the morphology of the Fe-rich phase. This modification alleviates stress concentration near the Fe-rich phase, thus preventing any degradation in the mechanical performance of the alloy. However, there is still phenomenon of eutectic silicon enrichment in the microstructure of the alloy. Compared to the untreated alloy, there is no significant change in the distribution of eutectic silicon phase. This suggests that while heat treatment fails to significantly alter the distribution of eutectic silicon, its primary mode of enhancing alloy performance lies in the modification of eutectic silicon morphology from lamellar or needle-like to an approximately spherical shape. Cai et al. [36] observed that heat treatment influences the spheroidization and dissolution of primary eutectic Si and Mg_2Si phases, resulting in improved tensile properties.

Image Pro Plus was used to measure the size of grain area (*A*). The following formula was used to calculate the grain size (equivalent grain diameter, *D*), and the results of grain size are shown in Fig. 8.

$$D = 2\sqrt{A/\pi}$$

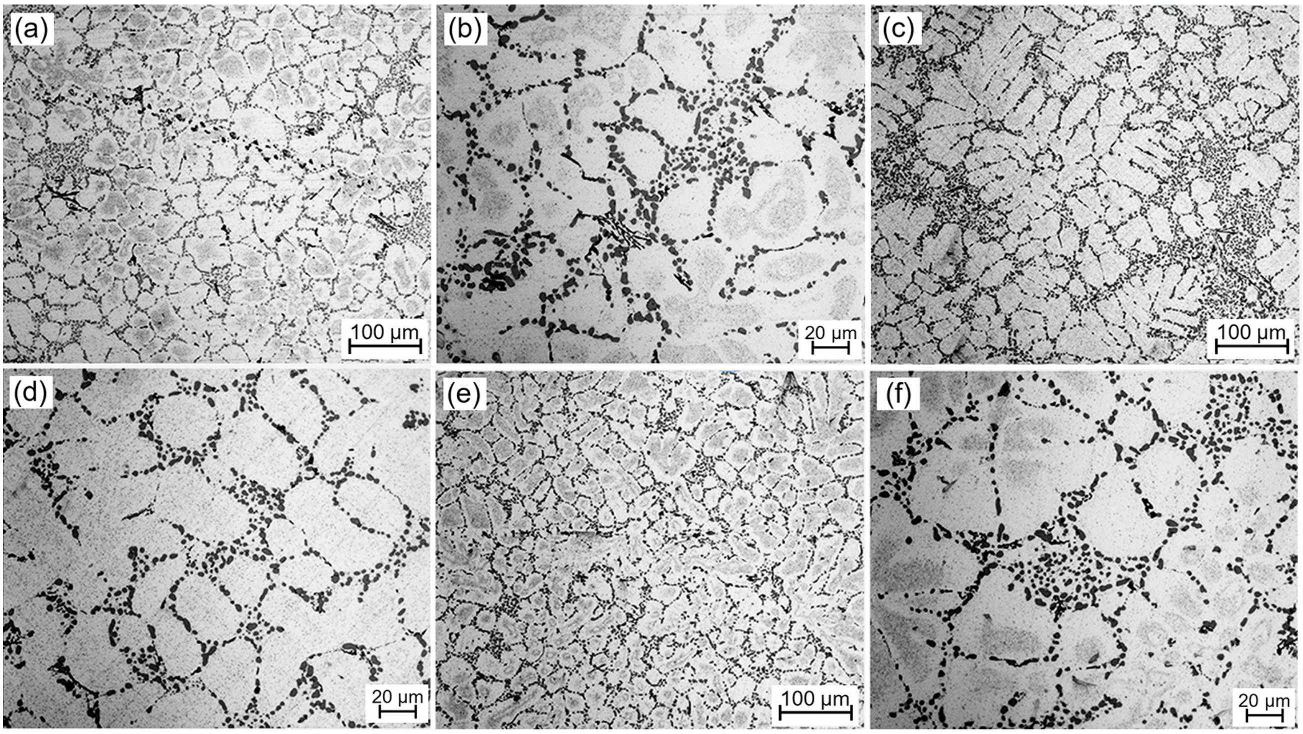

Fig. 6: Microstructure of the alloy at different magnification levels treated by an aging temeperature of 140 °C and varing aging times: (a, b) 3.5 h; (c, d) 4.5 h; (e, f) 5.5 h

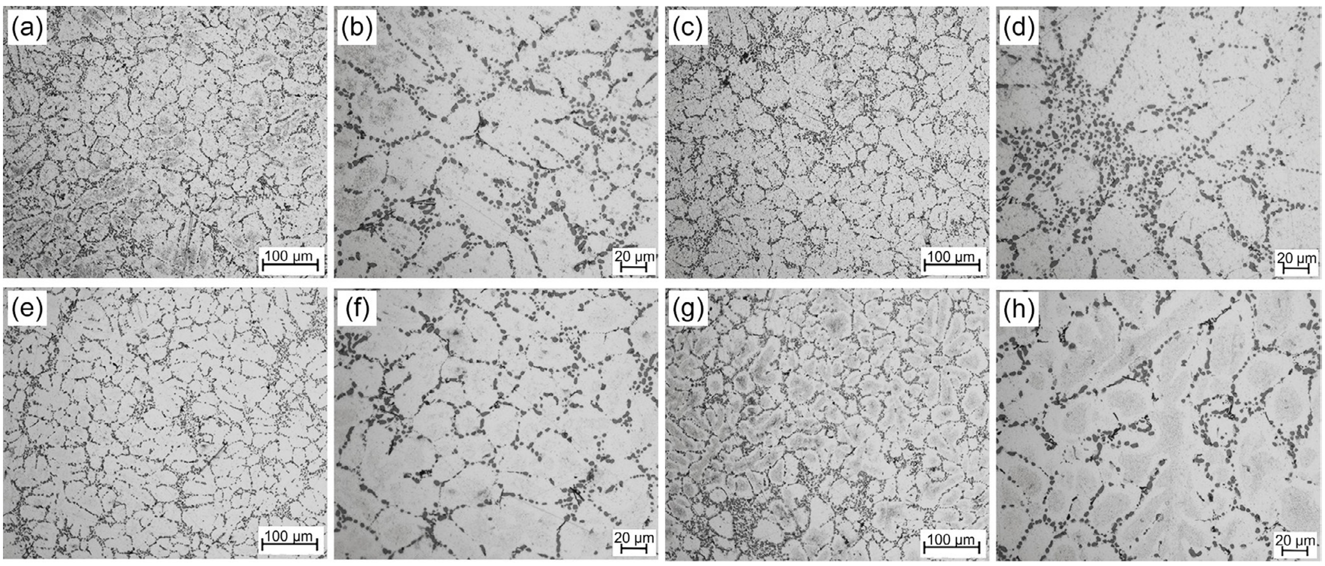

Fig. 7: Microstructure of the alloy at different magnification levels treated by an aging time of 5.5 h and varing aging temperatures: (a, b) 140 °C; (c, d) 150 °C; (e, f) 160 °C; (g, h) 170 °C

As depicted in Fig. 8, the grain size increases with prolonged aging time. Upon reaching an aging time of 5.5 h, the grain size exhibits a 20.6% increase compared to that of 4.5 h. An excessively extended aging time will lead to coarsening of the grains, and thus, the duration of the aging time should be controlled. With increasing aging temperatures, the equivalent grain size of the alloy initially decreases before rising, attaining its minimum at 160 °C, with an equivalent grain size of 33.8 μm. Initially, this decline may be attributed to the heightened formation of the Mg_2Si phase, influencing recrystallization nucleation and refining the aluminum matrix grains. However, as the aging temperature continues to rise, the solubility of the Mg_2Si phase increases, accelerating grain growth and diminishing the strengthening effect.

The SEM images of the alloy after different aging times are shown in Fig. 9, and the corresponding EDS point scanning results are summarized in Table 3. It is evident that in the microstructure of the heat-treated recycled aluminum alloy,

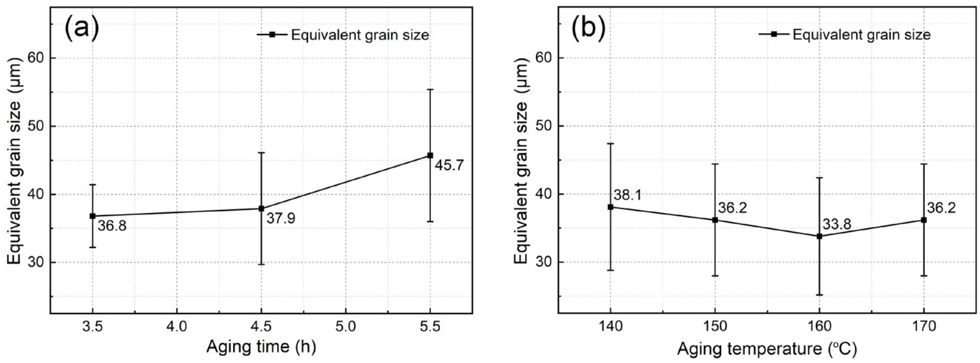

Fig. 8: Variation of equivalent grain size in the alloy treated by different aging parameters: (a) varing aging times at an aging temperature of 140 °C; (b) varing aging temperatures at an aging time of 5.5 h

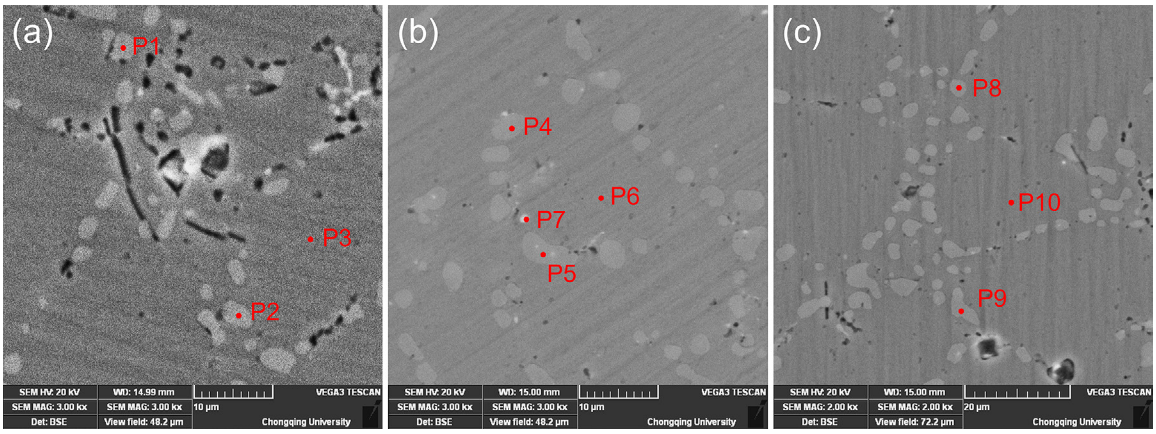

Fig. 9: SEM images of the alloy treated at an aging temperature of 140 °C for different aging times: (a) 3.5 h; (b) 4.5 h; (c) 5.5 h

Table 3: EDS point scanning results of alloys treated at an aging temperature of 140 °C for different aging times (wt.%)

Point	Al	Mg	Si	Ti	Fe
Point 1	40.98	0.28	58.31	0.04	0.39
Point 2	32.38	0.08	66.60	0.61	0.33
Ponit 3	97.16	0.75	1.76	0.25	0.08
Point 4	32.47	0.01	66.90	0.15	0.47
Point 5	34.75	0.12	64.49	0.58	0.06
Ponit 6	97.96	0.62	1.12	0.21	0.10
Point 7	85.34	0.14	7.26	0.11	7.15
Point 8	34.26	0.03	65.09	0.55	0.07
Ponit 9	28.90	0.23	70.57	0.02	0.28
Ponit 10	98.30	0.41	0.88	0.17	0.24

the nearly spherical particles present are eutectic silicon phase. There is a discernible reduction in the size of these eutectic silicon particles as the aging time prolongs, indicating that appropriately extending the aging time can change the morphology of the eutectic silicon phase, thereby mitigating its adverse impact on the alloy matrix. Furthermore, the scanning results from Point 7 reveal the presence of small white particles, which identified as iron-rich phases. Notably, the morphology of the particles in Fig. 9(c) differs significantly from that in as-cast alloys, indicating the modifying effect exerted by heat treatment on the iron-rich phase.

The strain-stress curves of the alloy after different aging times and aging temperatures are illustrated in Fig. 10. In comparison to the as-cast recycled aluminum alloy, the T6 heat-treated alloy exhibits significant improvements in both tensile strength and yield strength. Figure 10(a) indicates that the optimal tensile curve is attained at an aging temperature of 140 °C for an aging time of 5.5 h. However, there is minimal impact of aging time on the tensile strength of the alloy. From Fig. 10(b), it is evident that the impact of different aging temperatures on the alloy varies significantly. Therefore, it can be inferred that the aging temperature plays a crucial role in determining the tensile properties of the alloy.

Figure 11 illustrates the specific tensile properties of the alloy under varying aging times and temperatures, including tensile strength, yield strength, and elongation. In Figs. 11(a), (c), and (e), it is evident that as aging time increases, both tensile strength and yield strength demonstrate a rising trend, reaching peaks of 271.7 MPa and 222 MPa, representing increments of 45.1% and 130%, respectively compared to the as-cast alloy. This increase in strength can be attributed to solution aging strengthening, where an extended aging time leading to the generation of more Mg_2Si particles within the α-Al matrix, which can been observed from Fig. 9. Thereby, this enhances both the tensile and yield strength. Conversely, the elongation of the alloy exhibits an inverse trend. As

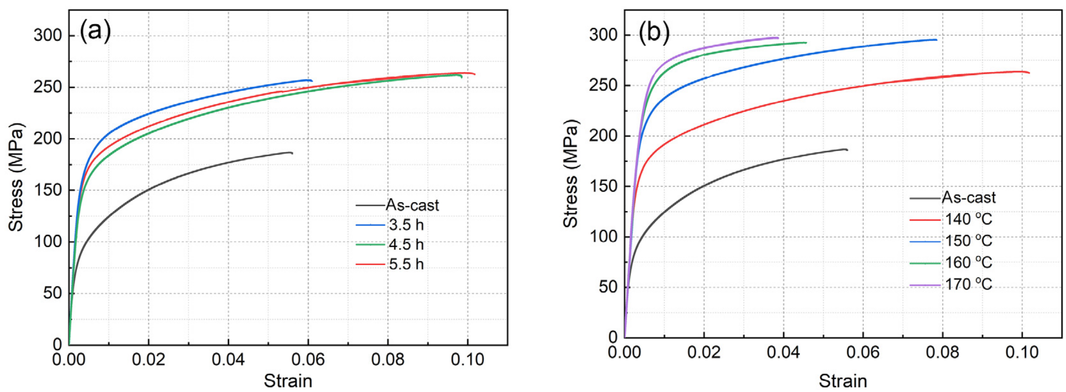

Fig. 10: Tensile stress-strain curves of the alloy treated by different aging parameters: (a) varing aging times with an aging temperature of 140 °C; (b) varing aging temperatures with an aging time of 5.5 h

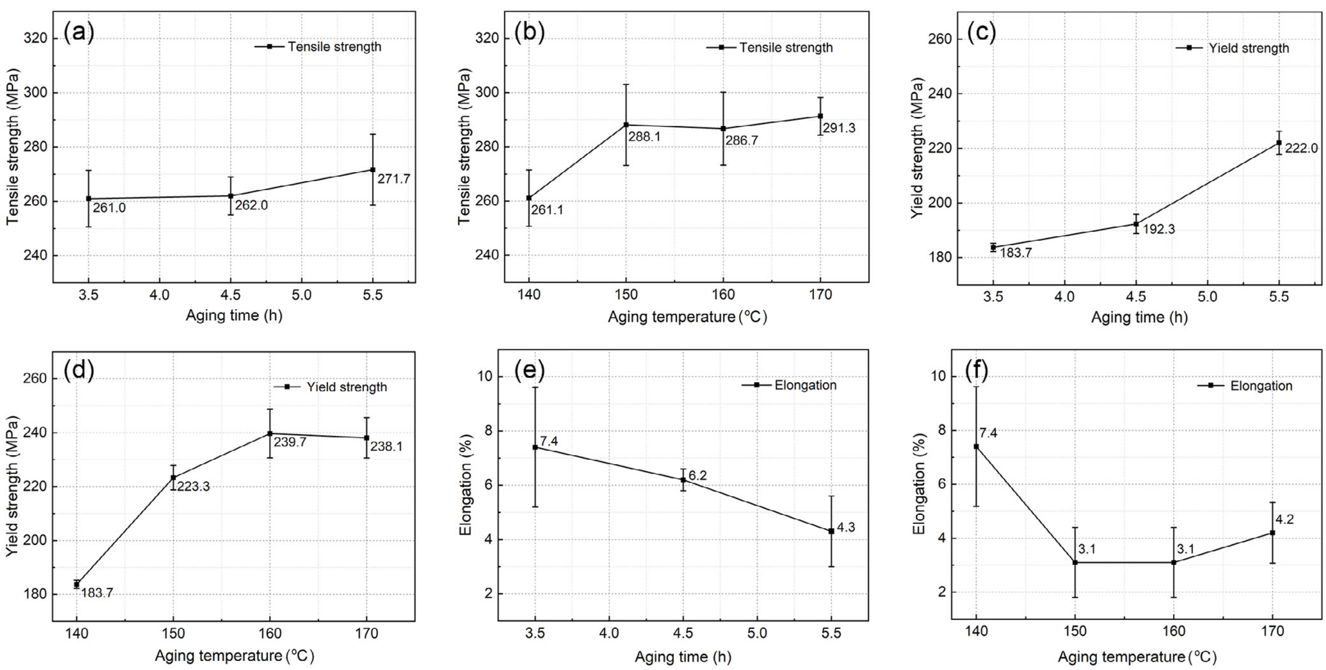

Fig. 11: Variation of tensile strength (a, b), yield strength (c, d), and elongation (e, f) of the alloy treated by different aging parameters: (a, c, e) varing aging times with an aging temperature of 140 °C; (b, d, f) varing aging temperatures with an aging time of 5.5 h

aging time extends from 3.5 h to 5.5 h, the alloy's elongation decreases by 41.9%, potentially due to non-uniform growth and deterioration in the roundness of Mg_2Si phases.

Figures 11(b), (d), and (f) reveal that the significant enhancements in both tensile and yield strength of the alloy following T6 heat treatment, with peak values at 291.3 MPa and 238.1 MPa, respectively. These values represent remarkable increases of 1.6 and 2.5 times compared to the as-cast alloy. However, there is a notable trade-off as the elongation decreases by 35.4% compared to the as-cast state. The tensile strength exhibits an upward trend with increasing aging temperature, plateauing at around 290 MPa. Specifically, a temperature rise from 140 °C to 150 °C results in a 10.8% increase in tensile strength. Similarly, the yield strength follows a similar pattern, peaking at 160 °C, beyond which further temperature increments yield no significant improvements. Interestingly, the elongation initially decreases with aging temperature, reaching its apex of 7.4% at the lowest aging temperature of 140 °C. However, a subsequent temperature increase from 140 °C to 150 °C induces a significant 56.3% reduction in elongation, possibly attributable to nonuniform growth of the Mg_2Si phase, which can be seen from Figs. 7(a–d). This observation aligns with findings by Pezda [37], who noted a similar trend in hypoeutectic Al-Si-Mg alloy, where lower aging temperatures (165 °C) contributed favorably to the increase in tensile strength, but it concurrently restricted elongation. Therefore, the optimal aging treatment parameters are an aging time of 5.5 h and an aging temperature of 170 °C, under which the alloy samples exhibit a tensile strength of 291.3 MPa, a yield strength of 238.1 MPa, and an elongation of 4.2%.

4 Conclusions

In this study, the optimal iron content was determined by comparing the microstructure and tensile properties of the alloys with varying iron content. The effects of aging temperatures and aging times on the microstructure and mechanical properties of the newly designed recycled aluminum alloy were investigated. The main findings can be summarized as follows:

(1) The optimal iron content is 0.2wt.% and heat treatment parameters for the newly designed recycled aluminum alloy are the solution treatment at 535 °C for 5 h, followed by an aging treatment at 170 °C for 5.5 h. After the optimal T6 heat treatment, the recycled aluminum alloy exhibits tensile strength, yield strength, and elongation, measuring at 291 MPa, 238 MPa, and 4.2%, respectively.

(2) As the iron content increases, the size of the iron-rich phase in the alloy increases. When the iron content is 0.2wt.%, the π-AlSiMgFe phase presents in a Chinese character shape. When the iron content is 0.3wt.%, the π-AlSiMgFe phase appears skeletal. When the iron content reaches 0.4wt.%, the needle-like β-AlFeSi phase and π-AlSiMgFe phase with Chinese character shape or skeleton-like shape grow intertwined.

(3) The addition of Sr and Mn, along with and the effect of heat treatment, has transformed the morphology of eutectic phase in the alloy from needle-like or plate-like to a globular shape. It alleviated the cracking effect of eutectic Si phase on the aluminum matrix.

(4) With increasing aging time, the equivalent grain size, tensile strength, and yield strength increase, while the elongation decrease. With increasing aging temperature, the tensile and yiled strength increase, while the equivalent grain size and elongation derease at first and then increase.

Acknowledgment

The authors would like to acknowledge the support from funded project: Key Industrial R & D Projects of Chongqing Technology Innovation and Application Demonstration (cstc2020jscx-dxwtBX0023).

Conflict of interest

The authors declare that they have no known competing financial interests or personal relationships that could have appeared to influence the work reported in this paper.

References

[1] Wang K, Li W, Xu W, et al. Simultaneous improvement of thermal conductivity and strength for commercial A356 alloy using strontium modification process. Met. Mater. Int., 2021, 27: 4742–4756. https://doi.org/10.1007/s12540-020-00669-x

[2] Xu S P, Shi C S, Zhao N Q, et al. Microstructure and tensile properties of A356 alloy with different Sc/Zr additions. Rare Met., 2021, 40(9): 2514–2522. https://doi.org/10.1007/s12598-020-01529-8

[3] Ozturk I, Agaoglu G H, Erzi E, et al. Corrosion behavior of B and Ti grain-refined Sr-modified A356. J. Mater. Eng. Perform., 2018, 27: 5197–5204. https://doi.org/10.1007/s11665-018-3657-3

[4] Niu G D, Wang J, Li J P, et al. Characterization of in-situ reinforced $(Al,Si)_3(Ti,Ce)$ precipitates in T6 treated A356-0.3wt.%Ce-1.5vol.%TiCN composite and its effects on mechanical properties. Mater. Charact., 2022, 185: 111756. https://doi.org/10.1016/j.matchar.2022.111756

[5] Song L Y, Liu H X, Nie S N, et al. Microstructure and fracture behavior of Al-Si-Mg alloy prepared with recycled alloy. Materwiss. Werksttech., 2019, 50: 462–470. https://doi.org/10.1002/mawe.201800041

[6] Lu H Z, Hou Z, Ma M T, et al. Effect of Fe-content on the mechanical properties of recycled Al alloys during hot compression. Metals, 2017, 7(7): 262. https://doi.org/10.3390/met7070262

[7] Daoud A, Abou El-Khair M T, Fairouz F, et al. Compressive behavior of 7075 Al-SiO_2 waste particle composite foams produced with recycled aluminum cans. J. Mater. Eng. Perform., 2020, 29: 2978–2990. https://doi.org/10.1007/s11665-020-04858-y

[8] Zhou B, Liu B, Zhang S, et al. Microstructure evolution of recycled 7075 aluminum alloy and its mechanical and corrosion properties. J. Alloys Compd., 2021, 879: 160407. https://doi.org/10.1016/j.jallcom.2021.160407

[9] Damgaard A, Larsen A W, Christensen T H. Recycling of metals: Accounting of greenhouse gases and global warming contributions. Waste Manag. Res., 2009, 27: 773–780. https://doi.org/10.1177/0734242X09346838

[10] Yasui S, Tsujimoto M, Itoh K, et al. Quenching of a photosensitized dye through single-electron transfer from trivalent phosphorus compounds. J. Org. Chem., 2000, 65: 4715–4720. https://doi.org/10.1021/jo000448i
[11] Wang Y, Xu H, Hu M, et al. Enhanced mechanical properties of a chip-based Al-Si-Cu-Fe alloy with an in-situ emulsion decomposition recycled by solid-state processing. Results Phys., 2019, 12: 718–724. https://doi.org/10.1016/j.rinp.2018.12.036
[12] Ragab A E, Taha M A, Abbas A T, et al. Effect of extrusion temperature on the surface roughness of solid state recycled aluminum alloy 6061 chips during turning operation. Adv. Mech. Eng., 2017, 9: 1–11, https://doi.org/10.1177/1687814017734152
[13] Reis A A Ô, De Oliveira J R, De Oliveira R M, et al. Thixoforging of Al-3.8% Si alloy recycled from aluminum cans. Mater. Sci. Eng. A, 2014, 607: 219–225. https://doi.org/10.1016/j.msea.2014.03.129
[14] Zhu X, Blake P, Dou K, et al. Strengthening die-cast Al-Mg and Al-Mg-Mn alloys with Fe as a beneficial element. Mater. Sci. Eng. A, 2018, 732: 240–250. https://doi.org/10.1016/j.msea.2018.07.005
[15] Jin L, Liu K, Chen X G. Evolution of Fe-rich intermetallics in Al-Si-Cu 319 cast alloy with various Fe, Mo, and Mn contents. Metall. Mater. Trans. B: Process Metall. Mater. Process. Sci., 2019, 50: 1896–1907. https://doi.org/10.1007/s11663-019-01584-2
[16] Chanyathunyaroj K, Patakham U, Kou S, et al. Microstructural evolution of iron-rich intermetallic compounds in scandium modified Al-7Si-0.3Mg alloys. J. Alloys Compd., 2017, 692: 865–875. https://doi.org/10.1016/j.jallcom.2016.09.132
[17] Kaiser M S, Towsif A, Reaz Ahmed S. Effect of post-weld thermal treatment on mechanical properties of welded aluminum-alloy engine head. J. Mater. Eng. Perform., 2017, 26: 4148–4154. https://doi.org/10.1007/s11665-017-2846-9
[18] Chen Y, Chen H, Zhu M, et al. Elements loss analysis based on spectral diagnosis in laser-arc hybrid welding of aluminum alloy. Int. J. Mod. Phys. B, 2017, 31: 1–5. https://doi.org/10.1142/S0217979217440362
[19] Wang Q, Hao Q, Yu W. Effect of strontium modification on porosity formation in A356 alloy. Int. J. Met., 2019, 13: 944–952. https://doi.org/10.1007/s40962-018-00300-1
[20] Timpel M, Wanderka N, Schlesiger R, et al. The role of strontium in modifying aluminium-silicon alloys. Acta Mater., 2012, 60: 3920–3928. https://doi.org/10.1016/j.actamat.2012.03.031
[21] Pramod S L, Ravikirana, Rao A K P, et al. Effect of Sc addition and T6 aging treatment on the microstructure modification and mechanical properties of A356 alloy. Mater. Sci. Eng. A, 2016, 674: 438–450. https://doi.org/10.1016/j.msea.2016.08.022
[22] Qiu C, Miao S, Li X, et al. Synergistic effect of Sr and La on the microstructure and mechanical properties of A356.2 alloy. Mater. Des., 2017, 114: 563–571. https://doi.org/10.1016/j.matdes.2016.10.061
[23] Haskel T, Verran G O, Barbieri R, et al. Effects of strontium addition and T6 heat treatment on uniaxial fatigue of A356 aluminum alloy: Fatigue life and cyclic behavior. Fatigue Fract. Eng. Mater. Struct., 2022, 45: 2159–2173. https://doi.org/10.1111/ffe.13721
[24] Yan W, Fu G, Xu Y, et al. Effect of Sr addition on the microstructure and properties of the A356 Al alloy. Mater. Tehnol., 2021, 55: 443–448. https://doi.org/10.17222/mit.2020.038
[25] Haskel T, Verran G O, Barbieri R. Rotating and bending fatigue behavior of A356 aluminum alloy: Effects of strontium addition and T6 heat treatment. Int. J. Fatigue, 2018, 114: 1–10. https://doi.org/10.1016/j.ijfatigue.2018.04.012
[26] Wu H, Zheng Z K, Li W C, et al. Effect of retrogression and re-aging treatment on properties and microstructure of a new type of Al-Zn-Mg-Er-Zr alloy. J. Mater. Eng. Perform., 2022, 31: 4282–4293. https://doi.org/10.1007/s11665-021-06557-8
[27] Bayraktar Ş, Demir O. Processing of T6 heat-treated Al-12Si-0.6Mg alloy. Mater. Manuf. Process., 2020, 35: 354–362. https://doi.org/10.1080/10426914.2020.1732412
[28] Zheng Y, Luo B, He C, et al. Effect of aging time on microstructure evolution and corrosion behavior of an Al-Mg-Si alloy. Mater. Res. Express, 2019, 6(11): 116582. https://doi.org/10.1088/2053-1591/ab4bec
[29] Geetha B, Ganesan K. The effects of ageing temperature and time on mechanical properties of A356 aluminium cast alloy with red mud addition and treated by T6 heat treatment. Mater. Today Proc., 2015, 2: 1200–1209. https://doi.org/10.1016/j.matpr.2015.07.032
[30] Tunçay T, Bayoğlu S. The effect of iron content on microstructure and mechanical properties of A356 cast alloy. Metall. Mater. Trans. B, 2017, 48: 794–804. https://doi.org/10.1007/s11663-016-0909-1
[31] Yi J Z, Gao Y X, Lee P D, et al. Effect of Fe-content on fatigue crack initiation and propagation in a cast aluminum-silicon alloy (A356-T6). Mater. Sci. Eng. A, 2004, 386: 396–407. https://doi.org/10.1016/j.msea.2004.07.044
[32] Gupta M, Ling S. Microstructure and mechanical properties of hypo/hyper-eutectic Al-Si alloys synthesized using a near-net shape forming technique. J. Alloys Compd., 1999, 287: 284–294. https://doi.org/10.1016/S0925-8388(99)00062-6
[33] Lu L, Dahle A K. Iron-rich intermetallic phases and their role in casting defect formation in hypoeutectic Al-Si alloys. Metall. Mater. Trans. A, 2005, 36: 819–835. https://doi.org/10.1007/s11661-005-0196-y
[34] Sweet L, Zhu S M, Gao S X, et al. The effect of iron content on the iron-containing intermetallic phases in a cast 6060 aluminum alloy. Metall. Mater. Trans. A, 2011, 42: 1737–1749. https://doi.org/10.1007/s11661-010-0595-6
[35] Karabulut C, Malkoç G, Kaya A Y, et al. Influence of different Fe levels on mechanical properties of AlSi7Mg0.3 aluminum casting alloys. Int. J. Met., 2023, 18: 3081–3094. https://doi.org/ 10.1007/s40962-023-01227-y
[36] Cai Q, Mendis C L, Chang I T H, et al. Effect of short T6 heat treatment on the microstructure and the mechanical properties of newly developed die-cast Al-Si-Mg-Mn alloys. Mater. Sci. Eng. A, 2020, 788: 139610. https://doi.org/10.1016/j.msea.2020.139610
[37] Pezda J. Influence of heat treatment parameters on the mechanical properties of hypoeutectic Al-Si-Mg alloy. Metalurgija, 2014, 53: 221–224